

Theranostic Nanoparticles Loaded with Imaging Probes and Rubrocurcumin for Combined Cancer Therapy by Folate Receptor Targeting

Diego Alberti,^[a] Nicoletta Protti,^[b, c] Morgane Franck,^[a] Rachele Stefania,^[a] Silva Bortolussi,^[b, c] Saverio Altieri,^[b, c] Annamaria Deagostino,^[d] Silvio Aime,^[a] and Simonetta Geninatti Crich^{*[a]}

The combination of different therapeutic modalities is a promising option to combat the recurrence of tumors. In this study, polylactic and polyglycolic acid nanoparticles were used for the simultaneous delivery of a boron–curcumin complex (RbCur) and an amphiphilic gadolinium complex into tumor cells with the aim of performing boron and gadolinium neutron capture therapy (NCT) in conjunction with the additional antiproliferative effects of curcumin. Furthermore, the use of Gd complexes allows magnetic resonance imaging (MRI) as-

essment of the amount of B and Gd internalized by tumor cells. Poly(lactic-co-glycolic acid) (PLGA) nanoparticles were targeted to ovarian cancer (IGROV-1) cells through folate receptors, by including in the formulation a PEGylated phospholipid functionalized with the folate moiety. NCT was performed on IGROV-1 cells internalizing 6.4 and 78.6 $\mu\text{g g}^{-1}$ of ^{10}B and ^{157}Gd , respectively. The synergic action of neutron treatment and curcumin cytotoxicity was shown to result in a significant therapeutic improvement.

Introduction

In recent years, much effort has been devoted to the use of combinations of different therapeutic modalities as possible strategies to treat cancer.^[1] This relies on the evidence that although a large majority of chemotherapeutic protocols and radiotherapies can considerably decrease tumor masses, they often fail to effect complete regression, as shown by a high number of tumor recurrence cases.^[2] Moreover, the time-dependent development of chemoresistance and radioresistance by a minor cell population within the tumor and the nonspecific toxicity toward normal cells are other major limitations of standard therapies.^[2,3] There is now an approved view that complete tumor regression can be achieved by the combination of different therapeutic strategies, whereas a decrease in off-target toxicity can be tackled by developing target-specific drugs endowed with minimized adverse effects or by the use of a more specific radiotherapeutic protocol that is able to discriminate between healthy and cancerous cells.


Boron neutron capture therapy (BNCT) is an unconventional radiotherapy that combines low-energy neutron irradiation in the presence of boron-containing compounds at targeted cells. Neutrons are captured by the non-radioactive isotope ^{10}B , which decays into α particles and lithium nuclei, which in turn cause irreparable damage to the cell in which they were generated.^[4] The low range of the charged particles permits selective destruction of tumor cells without affecting adjacent healthy cells if ^{10}B atoms are selectively accumulated in the intracellular space of tumor cells. This makes BNCT a promising option for the treatment of infiltrating tumors and disseminated metastases that cannot be treated by methods requiring a precise localization of the tumor mass, such as surgery or conventional radiotherapy.^[5] It has been estimated that $\sim 10\text{--}30 \mu\text{g}$ of ^{10}B per gram of tumor mass are needed to deliver a therapeutic dose of radiation to the tumor mass using an irradiation time shorter than a hour, which does not exceed the tolerance dose in normal tissues.^[6] The delivery of boron should be as selective as possible to tumor cells in order to increase the amount of internalized B in neoplastic cells, while minimizing uptake in surrounding healthy tissues and permanence in blood, which could damage normal organs and vessels. Two BNCT drugs are currently available for clinical investigation, namely: 1) L-para-boronophenylalanine (BPA), which has been used in clinical trials to treat glioblastoma,^[7] recurrent head and neck cancer,^[8] and melanoma;^[9] and 2) sodium mercaptoundecahydro-closedodecaborate (BSH), which has been investigated for the treatment of malignant glioma.^[10] Despite their clinical use, both BPA and BSH show low cell targeting selectivity, and much effort has been made by several research groups to develop new and more selective boron delivery agents.^[11]

[a] Dr. D. Alberti, Dr. M. Franck, Dr. R. Stefania, Prof. S. Aime, Prof. S. Geninatti Crich
Department of Molecular Biotechnology and Health Sciences, University of Torino, via Nizza 52, 10126, Torino (Italy)
E-mail: simonetta.geninatti@unito.it

[b] Dr. N. Protti, Dr. S. Bortolussi, Prof. S. Altieri
Department of Physics, University of Pavia, via Bassi 6, 27100, Pavia (Italy)

[c] Dr. N. Protti, Dr. S. Bortolussi, Prof. S. Altieri
Nuclear Physics National Institute (INFN), University of Pavia, via Bassi 6, 27100, Pavia (Italy)

[d] Prof. A. Deagostino
Department of Chemistry, University of Torino, via P. Giuria 7, 10125, Torino (Italy)

 Supporting information and the ORCID identification number(s) for the author(s) of this article can be found under <http://dx.doi.org/10.1002/cmdc.201700039>.

In this study, the stable adduct formed by boric acid, curcumin, and oxalic acid (rubrocurcumin)^[12] has been used to combine BNCT with the anticancer activity of curcumin. Curcumin is a natural polyphenolic compound that has a wide range of pharmacological activities.^[13] It has been proposed as a therapeutic agent, as it has shown antitumor activity *in vitro* and in animal models through the modulation or inhibition of multiple molecular pathways.^[14] Furthermore, it has been recently reported that curcumin acts as an efficient radiosensitizer through the upregulation of genes responsible for cell death.^[15] Another important property is that, unlike other known chemotherapeutic compounds, curcumin does not damage normal cells,^[16] and in some cases curcumin has also been shown to protect healthy organs such as liver, kidney, oral mucosa, and heart from chemotherapy and radiotherapy-induced toxicity.^[15] The formation of stable red complexes between B and curcumin has been exploited for the spectrophotometric detection of trace amounts of B in various media, including biological materials (e.g., foodstuffs, plants, and blood plasma), fresh and sea water, soil, iron and steel, as well as material relevant to nuclear technology.^[17] Moreover, promising medicinal applications of metal–curcumin complexes have been reported.^[17e,18] The factor that limits the use of free curcumin and its complexes for tumor therapy is its low aqueous solubility, which in turn limits its bioavailability when administered orally. To address this issue, nanotechnology-based carriers^[19] have been recently proposed for selective delivery to tumor sites along with appropriate curcumin functionalization, e.g., with poly(ethylene glycol) (PEG) chains.^[20]

Poly(lactic-co-glycolic acid) (PLGA) is one of the most effective biodegradable polymeric nanoparticles (NPs). It has been approved by the US Food and Drug Administration (FDA) as a drug delivery system owing to its controlled and sustained-release properties, low toxicity, and biocompatibility with tissues and cells.^[21] In this study, curcumin–boron complexes (RbCur) have been loaded into folate-targeted PLGA nanoparticles (PLGA-NP-folate; Figure 1) together with an amphiphilic Gd-based magnetic resonance imaging (MRI) contrast agent (Gd-DOTAMA).^[22]

This novel theranostic agent allows 1) maximization of the selective uptake of B atoms from tumor cells by targeting the folate receptor α (FRA), and 2) the indirect quantification of B

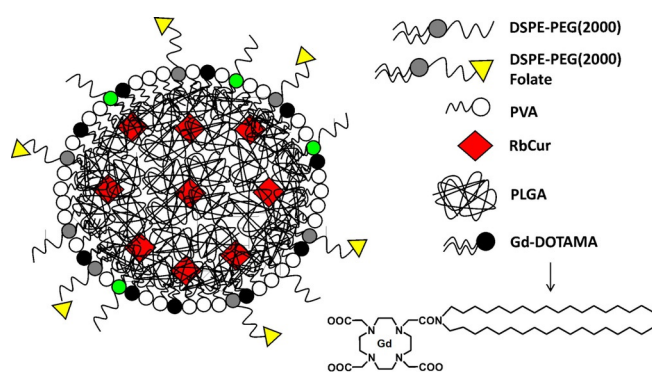


Figure 1. Schematic representation of folate-conjugated PLGA RbCur/Gd nanoparticles (PLGA-NP-folate).

distribution in the tumor and in other tissues via MRI response. To date, a noninvasive and repeatable *in vivo* B detection method remains unavailable, despite the well-established fact that measurement of local B concentrations is crucial to determine the optimal neutron irradiation time, to calculate the delivered radiation dose, and to evaluate the optimal irradiation time and duration.^[23] Moreover, ¹⁵⁷Gd is the second-most studied isotope to perform NCT, owing to its high cross-section for the capture of low-energy neutrons. The biological efficacy of Gd-based NCT is mainly due to the auger electron cascade induced by the internal conversion process that occurs in competition with γ -ray emission upon neutron capture from the ¹⁵⁷Gd isotope. The energy associated with auger electrons is 0.6% of the total emitted energy (7.94 MeV). Despite their low energy, these electrons may give strong cytotoxic effects if the ¹⁵⁷Gd nuclei are in close proximity to cellular DNA.^[5,24] In addition, Gd neutron capture also results in the release of long-range γ -rays which can also be advantageous in damaging resistant cells that did not internalize sufficient amounts of B/Gd to allow effective therapy.^[25] In this particular case, the location of the isotope is not critical with regard to the target cell, given the longer ranges of γ -rays. With the different mechanisms of action between BNCT and Gd-NCT, their combined use could be advantageous.^[26] One straightforward route involves the simultaneous administration of two NCT agents, one carrying ¹⁰B, the other ¹⁵⁷Gd, but this approach has the disadvantage that the uptake and distribution of the two atom types within the tumor may be quite different. In this study, ¹⁰B and ¹⁵⁷Gd were loaded into the same nanoparticle, thereby permitting their simultaneous distribution. The eventual increased dose through the ¹⁵⁷Gd capture reaction is analyzed and discussed herein.

Results and Discussion

The boron–curcumin dual agent rubrocurcumin (RbCur; Figure 2) was synthesized by reacting boric acid, curcumin,

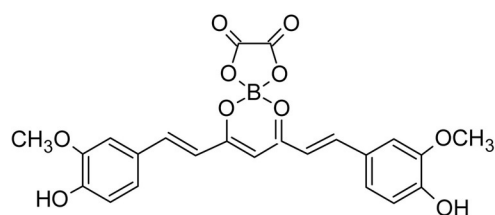


Figure 2. Structure of rubrocurcumin (RbCur).

and oxalic acid according to the procedure described by Sui et al.^[12b] The complex was characterized by UV/Vis spectrophotometry and by ¹H NMR spectroscopy. Figure 3 shows that after complex formation, the curcumin peak at 430 nm in the parent compound is shifted to 545 nm, where RbCur exhibits its maximum characteristic peak in ethanol.

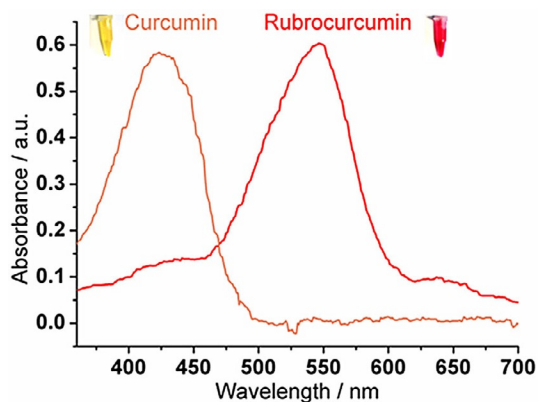


Figure 3. UV/Vis spectra of curcumin and rubrocurcumin acquired in ethanol at 10 μM .

Synthesis of PLGA nanoparticles

The methodology to obtain folate-conjugated and non-conjugated PLGA nanoparticles (PLGA-NP-folate and PLGA-NP-ctrl, respectively) was based on the oil/water (o/w) emulsion solvent extraction method.^[21] The organic phase was prepared by dissolving PLGA RG 503H, RbCur, Gd-DOTAMA, PEGylated phospholipid (DSPE-PEG(2000)methoxy) in 9:1 chloroform/methanol. For the preparation of PLGA-NP-folate, DSPE-PEG(2000)folate was added to the organic phase. The aqueous phase consisted of an aqueous solution of poly(vinyl alcohol) (PVA; 3% w/v). PVA is the most commonly used emulsifier for the preparation of these PLGA-based NPs because it yields particles that are relatively uniform, small, and easily re-dispersed in water.^[27] To obtain PLGA nanoparticles, the organic phase was added to the aqueous phase, and the mixture was sonicated for 5 min. The solidification of nanospheres was carried out by evaporation of the organic solvent from the o/w emulsion. The organic solvent was slowly removed by rotary evaporation for 2.5 h.

As reported in Table 1, the average hydrodynamic diameters of folate-targeted and un-targeted PLGA nanoparticles, determined by dynamic light scattering (DLS) measurements, show a homogeneous particle size distribution of ~ 150 nm, with a polydispersity index (PDI) of < 0.2 . The encapsulation yields of Gd-DOTAMA were significantly higher than for RbCur. An additional amount of curcumin (equal to the 43% w/w of the loaded RbCur) was found in the PLGA-NPs due to the partial dissociation of the RbCur complex during the loading protocol, as shown in the UV/Vis spectrum acquired immediately after its preparation (Figure 4). However, the remaining RbCur com-

plex encapsulated in the PLGA-NP was stable at 4 °C for two weeks, and all the subsequent experiments were performed within this time. The Gd complexes incorporated in PLGA-NP endowed the system with a high relaxivity ($26\text{--}28 \text{ mm}^{-1} \text{ s}^{-1}$ at 21.5 MHz, 25 °C) due to the partial exposure of the hydrophilic portion of the complex to the particle external surface and the partial water diffusion inside the polymeric material, which is inversely proportional to the PLGA-NP size.^[28]

Stability of PLGA nanoparticles

Through the use of inductively coupled plasma mass spectrometry (ICP-MS), the stability of PLGA nanoparticles was evaluated by measuring the release of B and Gd-DOTAMA from PLGA-NP-ctrl and PLGA-NP-folate. For this purpose, freshly prepared nanoparticle suspensions were dialyzed at 37 °C against 40 mL of HBS buffer for five days. Figure 5 shows that the amount of B released is $\sim 50\%$ after 6 h, and it increased to 60% after 24 h. In general, drug release depends on: 1) solubility, diffusion, and biodegradation of the matrix materials; 2) loading efficiency of the drug; and 3) size of the nanoparticles.^[29] The faster B release from the NP observed is a result of the relatively low stability of RbCur at 37 °C, with the consequent release of boric acid. The longitudinal water proton relaxation rate (R_1) measured over five days (Figure 5) showed only minor changes, suggesting a negligible release of Gd-DOTAMA over the observed time period. The relatively rapid release of B from the nanocage forced us to maintain a short incubation time (6 h) in the cell uptake experiments described in the following section.

Folate-targeting efficiency of PLGA-NPs and MRI visualization

Folate-conjugated PLGA-NPs have been tested for their efficacy in targeting human ovarian cancer (IGROV-1) cells overexpressing FRA.^[30] Folic acid is a typical cell-targeting agent given its high affinity for FRA, which is known to be overexpressed on the surface of many human cancer cells.^[31] The FRA captures folic acid from the extracellular milieu and transports it inside the cell via receptor-mediated endocytosis. There are various hypotheses concerning the precise mechanism of FRA-mediated trafficking into cells. As reported by Stella et al.^[32a] and Lu et al.,^[32b] folate-conjugated nanoparticles represent a multivalent form of the ligand folic acid. Because FRA are often found in clusters, conjugated nanoparticles could display a stronger

Table 1. Encapsulation yields of RbCur and Gd-DOTAMA, B and Gd concentrations in PLGA-NP-ctrl and PLGA-NP-folate solutions, and their size, relaxivity, and polydispersity indexes (PDI).

PLGA-NP	Yield [%] ^[a]		Relaxivity [$\text{mm}^{-1} \text{ s}^{-1}$] ^[a,b]	Size [nm] ^[a]	PDI	[B] [mM] ^[a]	[Gd] [mM] ^[a]
	Gd-DOTAMA	RbCur					
ctrl	71 \pm 7	12.6 \pm 4.3	26.1 \pm 1.7	144 \pm 3	0.099	0.8 \pm 0.3	0.7 \pm 0.1
folate	73 \pm 15	10.4 \pm 2.8	27.8 \pm 1.7	149 \pm 3	0.138	0.8 \pm 0.1	0.7 \pm 0.1

[a] Data are the mean \pm SD of four different experiments. [b] 21.5 MHz at 25 °C.

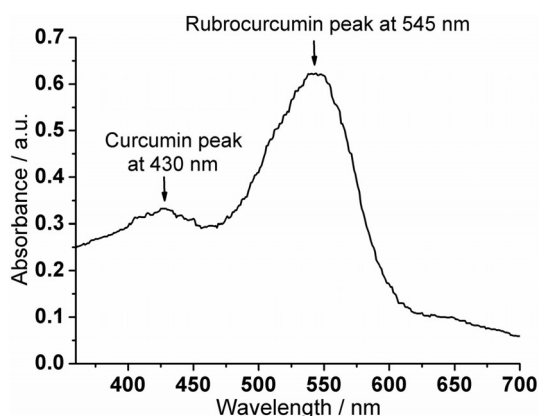


Figure 4. UV/Vis spectrum of RbCur loaded in PLGA-NP-ctrl acquired in ethanol.

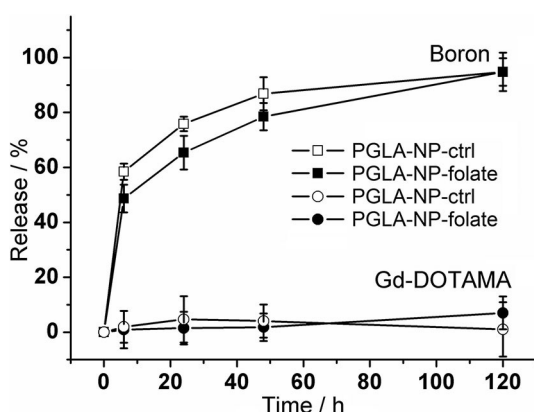


Figure 5. Evaluation of the stability of PLGA-NP-ctrl and PLGA-NP-folate loaded with RbCur and Gd-DOTAMA by measuring B and Gd concentrations in the NP solution over five days of dialysis at 37 °C in HBS. Data are the mean \pm SD of three different experiments.

multivalent interaction with the receptors, preventing their displacement by free folic acid.

The amounts of Gd and B internalized by IGROV-1 cells, measured by ICP-MS after 6 h incubation in the presence of increasing concentrations of PLGA-folate NPs were compared with the levels obtained with non-targeted NPs. Figure 6 shows that folate-targeted NPs reach complete saturation when their concentration in the incubation medium is $> 100 \mu\text{M}$ in Gd. This demonstrates a high affinity of folate-targeted NPs for the FRA and a negligible nonspecific cell binding of non-targeted NPs. The results obtained with IGROV-1 cells were compared with those obtained with human breast cancer (MCF-7) cells not expressing FRA,^[33] with healthy mouse mammary gland (NMuMg) cells and embryonic (BALB/C 3T3) fibroblasts using the same incubation protocol. Figure 6 shows that the internalization of PLGA-NP-folate by MCF-7, NMuMg, and 3T3 cells is negligible in the range of the concentrations tested. These observations suggest that the selectivity of PLGA-NP-folate is directed only to tumor cells overexpressing FRA and that their targeted intracellular delivery occurs via folate-receptor-mediated endocytosis.

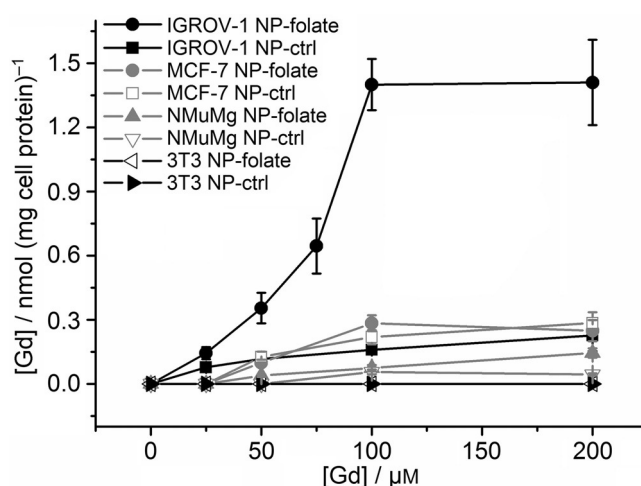


Figure 6. Uptake of PLGA-NP-ctrl and PLGA-NP-folate by IGROV-1, MCF-7, NMuMg, and 3T3 cells. Cells were incubated for 6 h at 37 °C in the presence of increasing concentrations of PLGA-NP-ctrl and PLGA-NP-folate (25–200 μM Gd). The amount of Gd taken up by cells was determined by ICP-MS, and values were normalized to the total cell protein content determined by Bradford assay. Data are the mean \pm SD of three different experiments.

The amounts of B and Gd internalized by IGROV-1 cells incubated with PLGA-NP-folate (100 μM Gd), as determined by ICP-MS, were found to be 6.4 and 78.6 $\mu\text{g g}^{-1}$ of B and Gd, respectively. Finally, MR images were acquired after incubating PLGA nanoparticles with IGROV-1 cells at a concentration of 100 μM Gd. As shown in Figure 7, the T_1 -weighted MR image acquired at 7 T of a phantom made of glass capillaries containing cell pellets, the recorded signal intensity (SI) of PLGA-NP-folate in IGROV-1 cells was significantly higher than for non-targeted NPs. This observation confirms the specific accumulation of folate-targeted NPs in tumor cells relative to control NPs.

- 1) Ctrl
- 2) PLGA-NP-ctrl
- 3) PLGA-NP-folate

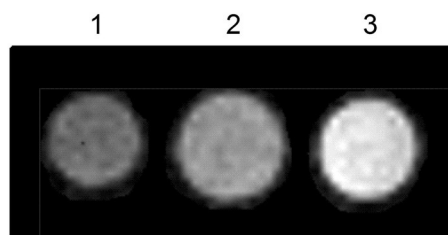


Figure 7. T_1 -weighted spin-echo MR image (measured at 7 T) of an agar phantom containing 1) untreated IGROV-1 cells, 2) cells incubated with PLGA-NP-ctrl, or 3) PLGA-NP-folate for 6 h at 37 °C at a Gd concentration of 100 μM .

To determine whether the combination of Gd/B-NCT and curcumin improves the treatment outcome (with respect to BNCT given as monotherapy), the clinically used B delivery agent boronophenylalanine (BPA; Figure 8A) was used as an alternative B source. For comparison, IGROV-1 cells were incubated for 3 h in the presence of increasing BPA concentrations

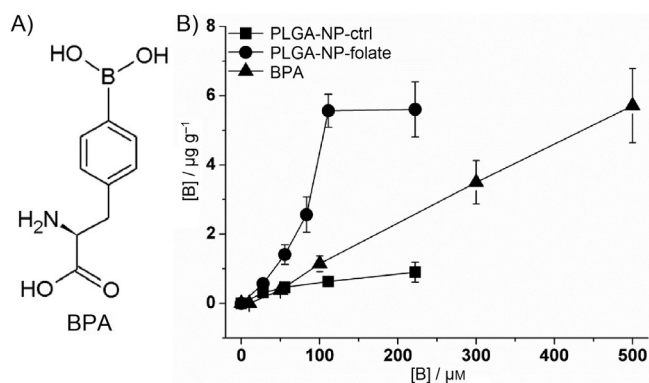


Figure 8. A) Structure of BPA. B) B internalization by IGROV-1 cells incubated in the presence of increasing BPA concentrations (10–500 μM B) for 3 h at 37 $^{\circ}\text{C}$ or with PLGA-NP-ctrl or PLGA-NP-folate (28–220 μM B) for 6 h at 37 $^{\circ}\text{C}$. Data are the mean \pm SD of three different experiments.

(10–500 μM B; Figure 8B). As expected, the internalization of PLGA-NP-folate (28–220 μM B) was significantly more efficient with respect to BPA uptake by IGROV-1 cells, and 6.4 $\mu\text{g g}^{-1}$ of B was reached after 6 h incubation. This amount of B is significantly lower than the minimum B concentration necessary to perform BNCT, but because the B was confined within the cells, this resulted in a sufficient concentration to produce an efficient neutron capture reaction. Only after incubation of BPA at 500 μM B, did the concentration of B internalized by cells reach 6.4 $\mu\text{g g}^{-1}$, whereas for PLGA-NP-folate, a fivefold lower concentration in the incubation medium was sufficient. This observation confirmed that the use of targeted nanoparticles allows the accumulation of B in tumor cells without the need for large doses of B carrier—doses that can enhance nonspecific uptake by healthy tissues.

BNCT treatment of IGROV-1 cells

To improve NCT performance, PLGA-NP-folate was prepared using Gd-DOTAMA and RbCur synthesized with ^{157}Gd (92.3%) and ^{10}B (99%) enriched isotopes, respectively. Three groups of IGROV-1 cells were considered: untreated cells irradiated only with thermal neutrons (2), BPA-treated cells then irradiated with neutrons (BNCT group) (4), and PLGA-NP-folate-treated cells then irradiated with neutrons (Gd-BNCT-group) (6). These were compared with the respective non-irradiated analogous (1), (3), and (5). Under these conditions, both treated cell groups were found to internalize the same amount of ^{10}B (6.4 $\mu\text{g g}^{-1}$). Groups (2), (4), and (6) were irradiated for 15 min in the thermal column of the TRIGA Mark II reactor at the University of Pavia (Reactor Power 30 kW).

IGROV-1 cells treated with PLGA-NP-folate [(5), (6)] and BPA [(3), (4)] were incubated for 6 h with PLGA-NP-folate (130 μM B) and 3 h with BPA 500 μM B, respectively. Figure 9A shows the percent of cells that survived neutron irradiation (2), (4), (6) with respect to the non-irradiated groups (1), (3), (5). We observed that the number of viable cells was significantly lower in the case of cells internalizing PLGA-NP-folate (6) than for cells internalizing BPA (4) (with the same amount of ^{10}B), both irradiated with neutrons as a consequence of the additional cy-

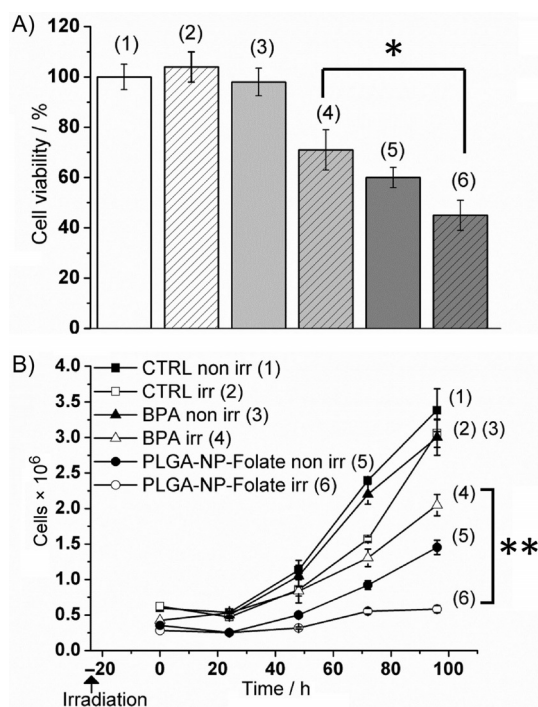


Figure 9. A) Percentage of IGROV-1 cells that survived BNCT treatment. (1) CTRL non-irradiated, (2) CTRL irradiated, (3) BPA non-irradiated, (4) BPA irradiated, (5) PLGA-NP-folate non-irradiated, (6) PLGA-NP-folate irradiated. Data are the mean \pm SD of three different experiments; * p = 0.0108, Student t -test. B) Proliferation curves of IGROV-1 cells re-plated one day after BNCT treatment. Data are the mean \pm SD of three different experiments; ** p = 0.0001, Student t -test.

totoxic effect of curcumin. The difference between groups (5) and (6) is less evident and statistically insignificant. Interestingly, the results changed by considering the proliferation rate of cells surviving irradiation; Figure 9B shows that both cells not irradiated (3) and irradiated (4) after BPA treatment, together with cells treated with PLGA-NP-folate (without irradiation) (5) rapidly restart proliferation, 72 h after irradiation, as the untreated controls (1). In contrast, cells treated with PLGA-NP-folate after neutron irradiation (6) showed a complete inhibition of proliferation.

The radiation dose absorbed by cells treated with BPA and PLGA-NP-folate reaching a ^{10}B concentration of 6.4 $\mu\text{g g}^{-1}$ ranges between 4.55 and 4.57 Gy. The total absorbed doses obtained in the presence of ^{157}Gd through PLGA-NP-folate increases very modestly by only 0.07%, assuming a non-nuclear Gd accumulation. Notably, 86% of the small increment observed with ^{157}Gd is due to the short-range internal conversion (IC) and auger electrons. Consequently, it cannot be excluded that a measurable increment in terms of cell death would be visible once the co-localization of ^{157}Gd nuclei and cell DNA is guaranteed. Finally, in the two NCT groups (cells exposed to BPA or PLGA-NP-folate), \sim 45% of the total dose is due to secondary radiation emitted in the neutron capture reaction of ^{10}B , while in the third irradiated group (neutron only) receiving \sim 2.5 Gy, up to 91% of the total dose is imparted by γ -rays coming from the neutron capture reaction of ^1H in the cell layer and from the photon background characterizing the irradiation position inside the thermal column.

Although the intracellular ^{157}Gd concentration was not sufficient to produce an increment in terms of cell damage after neutron irradiation, the presence of curcumin before and during neutron exposure resulted in an improved treatment outcome with respect to BNCT used as monotherapy with the same B concentration [$\mu\text{g g}^{-1}$] accumulated using BPA alone as B source. The presence of curcumin increased cell mortality and significantly decreased cell proliferation of the surviving cells, despite the B concentration being below the established threshold for effective BNCT treatment ($10\text{--}30\ \mu\text{g g}^{-1}$). Due to the difficulties encountered in obtaining such high B concentrations, requiring patient perfusion with highly concentrated solutions of BPA for many hours, this result is fundamental to increase the competitiveness of BNCT relative to other conventional tumor treatment protocols.

Conclusions

In this work, the antitumor activity arising from Gd- and BNCT combined with curcumin was tested on IGROV-1 ovarian cancer cells, using an innovative folate-targeted PLGA nanoparticle containing both Gd and the curcumin–boron complex RbCur. This new nanoparticle has shown to be an efficient carrier that acts via folate receptors and can be exploited for the measurement of Gd and indirectly B concentrations by MRI, opening new perspectives in neutron capture applications.

Experimental Section

Materials: Curcumin, boric acid, oxalic acid, poly(D,L-lactide-co-glycolide) (PLGA) 50:50 (Resomer RG 503H), M_r 30–60 kDa and poly(vinyl alcohol) (Mowiol 4-88), M_r 31 kDa were provided by Sigma-Aldrich (St. Louis, MO, USA). DSPE-PEG(2000){1,2-distearoyl-*sn*-glycero-3-phosphoethanolamine-*N*-[methoxy(polyethylene glycol)-2000] ammonium salt} and DSPE-PEG(2000)folate {1,2-distearoyl-*sn*-glycero-3-phosphoethanolamine-*N*-[folate(polyethylene glycol)-2000] ammonium salt} were purchased from Avanti Polar Lipids (Alabaster, AL, USA). The lipophilic Gd-DOTAMA was synthesized according to a previously reported procedure.^[22]

Rubrocurcumin synthesis and characterization: A suspension of curcumin (369 mg, 1 mmol), boric acid (62 mg, 1 mmol), and oxalic acid (91 mg, 1 mmol) in 40 mL toluene was stirred and heated at reflux for 16 h using a Dean–Stark trap. For irradiation experiments, the naturally occurring boric acid was substituted with 99% ^{10}B -enriched (Sigma–Aldrich). After cooling, the red precipitate was collected and washed several times with toluene and ethyl acetate before drying under reduced pressure (261 mg, yield: 56%). UV: $\lambda_{\text{max}} = 545\ \text{nm}$; MS (ESI+): m/z : calcd for $\text{C}_{23}\text{H}_{19}\text{BO}_{10} [\text{M} + \text{H}]^+$ 466.1, found: 466.9. The compound showed sufficient purity (85%) determined by ^1H NMR spectroscopy, (600 MHz, $[\text{D}_6]$ acetone): $\delta = 3.93$ (s, 6H, OCH_3), 6.55 (s, 1H, CH), 6.96 (d, 2H, $J = 7.8\ \text{Hz}$, Ar), 7.07 (d, 2H, $J = 15.7\ \text{Hz}$, Ar), 7.42 (d, 2H, $J = 8.3\ \text{Hz}$, Ar), 7.51 (s, 2H, Ar), 8.11 (d, 2H, $J = 15.4\ \text{Hz}$, Ar), 8.83 ppm (br, OH) (Supporting Information). ^1H NMR spectra were acquired on a Bruker Avance 600 spectrometer (Bruker BioSpin, Ettlingen, Germany). Mass spectral analyses were performed with a Waters 3100 mass spectrometer in ESI(+) mode.

Synthesis of PLGA nanoparticles: Two different nanospheres were prepared: one targeted with folate and the other nontargeted and

used as control. Nanospheres were obtained using the oil-in-water emulsion solvent extraction method. Folate-targeted nanoparticles were prepared by dissolving 25 mg of PLGA, 1.2 mg of DSPE-PEG(2000)folate, 1 mg of DSPE-PEG(2000)methoxy, 3.2 mg of Gd-DOTAMA, and 6 mg of RbCur in 600 μL (9:1 $\text{CHCl}_3/\text{MeOH}$, phase 1); nontargeted nanoparticles were prepared by dissolving 25 mg of PLGA, 2.2 mg of DSPE-PEG(2000)methoxy, 3.2 mg of Gd-DOTAMA, and 6 mg of RbCur in 600 μL (9:1 $\text{CHCl}_3/\text{MeOH}$, phase 1). For both nanoparticles, phase 2 consisted of a 3% w/v aqueous solution of PVA (3 mL). Phase 1 was added dropwise into phase 2, and the obtained emulsion was sonicated (Bandelin Electronic, Berlin, Germany) in ice at 100% power for 5 min. The emulsion was immediately put into a rotary evaporator (740 Torr, 30 rpm) for 150 min to remove the organic solvent. After evaporation, the untrapped compounds were removed by dialysis (M_r cutoff: 14 kDa) at 4 °C in 1 L isotonic NaCl/HEPES buffer (HBS). Excess PVA was removed by washing the emulsion with a Vivaspin 20 filter (Sartorius AG, Göttingen, Germany; M_r cutoff: 1×10^6 Da), and at the end of the washing step a final volume of 2 mL was reached for all the nanoparticle suspensions considered. The amounts of Gd and B incorporated into PLGA nanoparticles were measured by inductively coupled plasma mass spectrometry (ICP-MS; element-2; ThermoFinnigan, Rodano (MI), Italy) after sample digestion performed with concentrated HNO_3 (70%, 1 mL) under microwave heating (Milestone MicroSYNTH Microwave Labstation). The amount of Gd was double checked by ^1H NMR R_1 measurement at 21.5 MHz, 25 °C (Stelar Spinmaster, Mede, Italy) of the mineralized complex solution (in 6 M HCl at 120 °C for 16 h). The hydrated mean diameter of nanoparticles was determined using a dynamic light scattering (DLS) Malvern Zetasizer 3000HS (Malvern, UK). All samples were analyzed at 25 °C in filtered (200 nm cutoff) HBS buffer (pH 7.4). The amounts of RbCur and curcumin loaded into the PLGA-NPs were determined by acquiring a UV/Vis spectrum in the range of 360–700 nm in EtOH. According to the calibration curve of RbCur ($y = 0.1303x - 0.015$ ($\mu\text{g mL}^{-1}$ at 545 nm)) and curcumin ($y = 0.15582x$ ($\mu\text{g mL}^{-1}$ at 430 nm)) the encapsulation yield was calculated with Equation (1):

$$\% \text{ Encapsulation} = (\text{RbCur}_{\text{encapsulated}} / \text{RbCur}_{\text{total}}) \times 100 \quad (1)$$

for which $\text{RbCur}_{\text{encapsulated}}$ is the amount of RbCur measured after the NP preparation, and $\text{RbCur}_{\text{total}}$ is the total amount of RbCur used to prepare the NP. Nanoparticles were stored in the dark at 4 °C until further analysis.

Stability of PLGA nanoparticles: To perform stability tests, 2.5 mL of PLGA-NP-ctrl and PLGA-NP-folate at a 0.2 mM Gd concentration in HBS buffer were dialyzed at 37 °C (M_r cutoff: 14 kDa) in 40 mL HBS for five days. At various time intervals, 200 μL of the dialyzed NP solution was taken to measure Gd and B concentrations. The 40 mL HBS buffer was refreshed at each drawing. The amounts of Gd and B were measured by ICP-MS. The percentage of Gd and B released was calculated with Equation (2):

$$\% \text{ Release} = \left(\frac{[\text{Gd}/\text{B}(t_0) - \text{Gd}/\text{B}(t_i)]}{\text{Gd}/\text{B}(t_0)} \right) \times 100 \quad (2)$$

for which $\text{Gd}/\text{B}(t_i)$ is the amount of Gd or B measured by ICP-MS inside the dialysis membrane at the various time intervals ($t = 0, 6, 24, 48,$ and $120\ \text{h}$), and $\text{Gd}/\text{B}(t_0)$ is the amount of Gd or B at the starting point ($t = 0$) of the stability test.

Cell culture and uptake experiments: The IGROV-1 human ovarian carcinoma cell line was kindly provided by Dr. Claudia Cabella

(Bracco Imaging, Colliere Giacosa, TO, Italy). IGROV-1 cells were cultured in RPMI (Lonza) supplemented with 10% (v/v) FBS, 2 mM glutamine, 100 U mL⁻¹ penicillin, and 100 U mL⁻¹ streptomycin. MCF-7 human breast cancer cells and BALB/C 3T3 murine embryo fibroblasts were obtained from the American Type Culture Collection (ATCC), and the NMuMg cell line, derived from a healthy mouse mammary gland, was kindly provided by Prof. Lollini PL (University of Bologna, Italy). MCF-7 cells were cultured in EMEM (Lonza) supplemented with 10% (v/v) FBS, 2 mM glutamine, 100 U mL⁻¹ penicillin, and 100 U mL⁻¹ streptomycin, 1 mM sodium pyruvate and nonessential amino acids, and 10 μg mL⁻¹ insulin (Sigma). NMuMg cells were cultured in RPMI (Lonza) supplemented with 10% (v/v) FBS, 2 mM glutamine, 100 U mL⁻¹ penicillin, 100 U mL⁻¹ streptomycin, and 10 μg mL⁻¹ insulin (Sigma). BALB/C 3T3 cells were cultured in DMEM (Lonza) supplemented with 10% (v/v) FBS, 4 mM glutamine, 100 U mL⁻¹ penicillin, and 100 U mL⁻¹ streptomycin. Cells were incubated at 37 °C in a humidified atmosphere of 5% CO₂. For the in vitro uptake experiments, 4.5 × 10⁵ IGROV-1, 6 × 10⁵ MCF-7, 4 × 10⁵ NMuMg, and 6 × 10⁵ BALB/C 3T3 cells were seeded in 6 cm diameter culture dishes. After 24 h, the IGROV-1 cell medium was removed and replaced with RPMI without folate to increase folate receptor expression. After another 24 h, all cells were incubated for 6 h in folate-free medium with increasing concentrations (25–200 μM in Gd) of PLGA-NP-ctrl or PLGA-NP-folate. At the end of incubation, cells were washed with ice-cold PBS (3 × 5 mL), detached with 0.05% trypsin and 0.02% EDTA in PBS. IGROV-1 cells were further transferred into glass capillaries for MRI analysis (see below). For the BPA uptake assays, 4.5 × 10⁵ IGROV-1 cells were seeded in 6 cm diameter culture dishes. After 48 h the medium was removed and replaced with EBSS buffer in the presence of increasing concentrations of BPA (10–500 μM B) for 3 h. At the end of incubation, cells were washed with ice-cold PBS (3 × 5 mL), detached with 0.05% trypsin and 0.02% EDTA in PBS. Finally, all cell samples were transferred to falcon tubes and sonicated at 30% power for 30 s on ice; total cell protein concentrations were determined by a commercial Bradford assay (Bio-Rad, Hercules, CA, USA). Gd and B content in the cell samples was determined by ICP-MS, and values were normalized to the protein content of each cell sample that was correlated to the number of cells by means of a calibration curve: [(mg protein)/(number of cells)]. The amounts of B and Gd [μg (g tissue)⁻¹] were thus calculated considering that 1 g of tissue contains 1 × 10⁹ cells.

Magnetic resonance imaging: MR images were acquired at 7 T on a Bruker Avance 300 spectrometer equipped with a Micro 2.5 microimaging probe (Bruker BioSpin, Ettlingen, Germany) using a birdcage resonator of 10 mm inner diameter. For recording MR images in vitro, cells were pelleted at the bottom of glass capillaries placed in a phantom embedded with high-gelling agarose (1% w/v in PBS). MR images were acquired using a standard T₁-weighted multi-slice spin-echo sequence, using the following parameters: TR/TE/NEX 250/4/6, resolution 78 μm, slice thickness 1 mm.

Cell irradiation: Eight flasks, three with IGROV-1 cells previously incubated for 6 h in the presence of PLGA-NP-folate, 130 μM B, three incubated for 3 h with BPA at 500 μM B, and two untreated control cells were irradiated in the thermal column of the TRIGA Mark II reactor at the University of Pavia, Italy. Cells incubated in the presence of PLGA nanoparticles and BPA were washed with cold PBS before irradiation. At the end of the irradiation, the medium was removed, replaced with fresh RPMI, and flasks were placed at 37 °C in a humidified atmosphere of 5% CO₂. The irradiation position was previously characterized from the point of view of neutron flux distribution by means of thin activation foils.^[34] At a reactor

power of 250 kW the thermal neutron flux in air at that position is (1.20 ± 0.10) × 10¹⁰ cm⁻² s⁻¹, while the epithermal and fast components are at least two orders of magnitude lower. The flux is roughly constant (< 1%) along the vertical direction, and thus the flasks were superposed and irradiated at the same time. The irradiation time was fixed at 15 min at a reactor power of 30 kW, corresponding to a thermal neutron fluence of 1.30 × 10¹² cm⁻².

Proliferation assays: The day after irradiation, cells were detached with 0.02% EDTA, and the trypan blue exclusion test for cell viability was performed. Then, ~6 × 10⁵ IGROV-1 cells from each differently treated flask were seeded in 10 cm diameter culture dishes. At days 1, 2, 3, and 4, cells were washed with PBS, detached with 0.05% trypsin and 0.02% EDTA in PBS and transferred into falcon tubes. Cells were then sonicated for 30 s at 30% power on ice, and the total cell protein concentration from cell lysates was determined by the Bradford method, using bovine serum albumin as a standard.

Acknowledgements

This research was funded by MIUR (PRIN 2012 code 2012SK7ASN), the AIRC Investigator Grant IG2013, and by the National Institute of Nuclear Physics (INFN), Italy, project "NETTUNO". This research was performed in the framework of the EU COST Action TD1004. The authors thank the staff of the Laboratory of Applied Nuclear Energy (LENA, University of Pavia) for their valuable support in neutron irradiation experiments.

Keywords: boron neutron capture therapy · curcumin · gadolinium · magnetic resonance imaging · oncology · poly(lactic-co-glycolic acid)

- [1] J. A. Kemp, M. S. Shim, C. Y. Heo, Y. J. Kwon, *Adv. Drug Delivery Rev.* **2016**, *98*, 3–18.
- [2] H. E. Barker, J. T. Paget, A. A. Khan, K. J. Harrington, *Nat. Rev. Cancer* **2015**, *15*, 409–425.
- [3] L. Gatti, F. Zunino, *Methods Mol. Med.* **2005**, *111*, 127–148.
- [4] A. H. Soloway, W. Tjarks, B. A. Barnum, F. G. Rong, R. F. Barth, I. M. Coddogni, J. G. Wilson, *Chem. Rev.* **1998**, *98*, 1515–1562.
- [5] a) E. C. C. Pozzi, J. E. Cardoso, L. L. Colombo, S. Thorp, A. Monti Hughes, A. J. Molinari, M. A. Garabalino, E. M. Heber, M. Miller, M. E. Itoiz, R. F. Aromando, D. W. Nigg, J. Quintana, V. A. Trivillan, A. E. Schwint, *Radiat. Environ. Biophys.* **2012**, *51*, 331–339; b) N. S. Hosmane, J. A. Maguire, Y. Zhu, M. Takagaki, *Boron and Gadolinium Neutron Capture Therapy for Cancer Treatment*, World Scientific Pub. Co. Inc., Singapore, **2012**.
- [6] a) R. F. Barth, *Appl. Radiat. Isot.* **2009**, *67*, S3–6; b) R. F. Barth, J. A. Coderre, M. G. Vicente, T. E. Blue, *Clin. Cancer Res.* **2005**, *11*, 3987–4002; c) M. F. Hawthorne, M. W. Lee, *J. Neurooncol.* **2003**, *62*, 33–45.
- [7] a) T. Kageji, S. Nagahiro, Y. Mizobuchi, K. Matsuzaki, Y. Nakagawa, H. Kumada, *J. Med. Invest.* **2014**, *61*, 254–263; b) C. M. van Rij, A. J. Wilhelm, W. A. Sauerwein, A. C. van Loenen, *Pharm. World Sci.* **2005**, *27*, 92–95; c) T. Yamamoto, K. Nakai, A. Matsumura, *Cancer Lett.* **2008**, *262*, 143–152.
- [8] a) Y. W. Liu, C. T. Chang, L. Y. Yeh, L. W. Wang, T. Y. Lin, *Appl. Radiat. Isot.* **2015**, *106*, 121–124; b) T. Aihara, N. Morita, N. Kamitani, H. Kumada, K. Ono, J. Hiratsuka, T. Harada, *Appl. Radiat. Isot.* **2014**, *88*, 12–15; c) L. Kankaanranta, T. Seppälä, H. Koivunoro, K. Saarilahti, T. Atula, J. Collan, E. Salli, M. Korttinen, J. Uusi-Simola, P. Välimäki, A. Mäkitie, M. Seppänen, H. Minn, H. Revitzer, M. Kouri, P. Kotiluoto, T. Seren, I. Auterinen, S. Savolainen, H. Joensuu, *Int. J. Radiat. Oncol. Biol. Phys.* **2012**, *82*, e67–e75.
- [9] P. R. Menéndez, B. M. Roth, M. D. Pereira, M. R. Casal, S. J. González, D. B. Feld, G. A. Santa Cruz, J. Kessler, J. Longhino, H. Blaumann, R. Jiménez

- Rebagliati, O. A. Calzetta Larriue, C. Fernández, S. I. Nieves, S. J. Liberman, *Appl. Radiat. Isot.* **2009**, *67*, S50–53.
- [10] R. F. Barth, M. G. Vicente, O. K. Harling, W. S. Kiger, 3rd, K. J. Riley, P. J. Binns, F. M. Wagner, M. Suzuki, T. Aihara, I. Kato, S. Kawabata, *Radiat. Oncol.* **2012**, *7*, 146–167.
- [11] a) V. M. Ahrens, R. Frank, S. Boehnke, C. L. Schütz, G. Hampel, D. S. Iffland, N. H. Bings, E. Hey-Hawkins, A. G. Beck-Sickinger, *ChemMedChem* **2015**, *10*, 164–172; b) S. Tachikawa, T. Miyoshi, H. Koganei, M. E. El-Zaria, C. Viñas, M. Suzuki, K. Ono, H. Nakamura, *Chem. Commun.* **2014**, *50*, 12325–12328.
- [12] a) G. S. Spicer, J. D. H. Strickland, *J. Chem. Soc.* **1952**, 4644–4650; b) Z. Sui, R. Salto, J. Li, C. Craik, P. R. Ortiz de Montellano, *Bioorg. Med. Chem.* **1993**, *1*, 415–422.
- [13] a) T. Esatbeyoglu, P. Huebbe, I. M. Ernst, D. Chin, A. E. Wagner, G. Rimbach, *Angew. Chem. Int. Ed.* **2012**, *51*, 5308–5332; *Angew. Chem.* **2012**, *124*, 5402–5427; b) B. B. Aggarwal, C. Sundaram, N. Malani, H. Ichikawa, *Adv. Exp. Med. Biol.* **2007**, *595*, 1–75.
- [14] a) M. López-Lázaro, *Mol. Nutr. Food Res.* **2008**, *52*, S103–S127; b) A. Sahabkar, A. F. Cicero, L. E. Simental-Mendía, B. B. Aggarwal, S. C. Gupta, *Pharmacol. Res.* **2016**, *107*, 234–242.
- [15] a) G. C. Jagetia, *Adv. Exp. Med. Biol.* **2007**, *595*, 301–320; b) D. Chendil, R. S. Ranga, D. Meigooni, S. Sathishkumar, M. M. Ahmed, *Oncogene* **2004**, *26*, 1599–1607.
- [16] C. Syng-Ai, A. L. Kumari, A. Khar, *Mol. Cancer Ther.* **2004**, *3*, 1101–1108.
- [17] a) M. R. Hayes, J. Metcalfe, *Analyst* **1962**, *87*, 956–969; b) J. W. Mair, Jr., H. G. Day, *Anal. Chem.* **1972**, *44*, 2015–2017; c) W. W. Choi, K. Y. Chen, *Am. Water Works Assoc.* **1979**, *71*, 153–157; d) M. A. Wimmer, H. E. Goldbach, *J. Plant Nutr. Soil Sci.* **1999**, *162*, 15–18; e) S. Wanninger, V. Lorenz, A. Subhan, F. T. Edelman, *Chem. Soc. Rev.* **2015**, *44*, 4986–5002.
- [18] S. Banerjee, A. R. Chakravarty, *Acc. Chem. Res.* **2015**, *48*, 2075–2078.
- [19] M. Z. Ahmad, S. A. Alkahtani, S. Akhter, F. J. Ahmad, J. Ahmad, M. S. Akhtar, N. Mohsin, B. A. Abdel-Wahab, *J. Drug Targeting* **2016**, *24*, 273–293.
- [20] M. K. Pandey, S. Kumar, R. K. Thimmulappa, V. S. Parmar, S. Biswal, A. C. Watterson, *Eur. J. Pharm. Sci.* **2011**, *43*, 16–24.
- [21] a) R. A. Jain, *Biomaterials* **2000**, *21*, 2475–2490; b) R. N. Mariano, D. Alberti, J. C. Cutrin, S. Geninatti Crich, S. Aime, *Mol. Pharm.* **2014**, *11*, 4100–4106; c) L. N. Turino, R. N. Mariano, S. Boimvaser, J. A. Luna, *J. Pharm. Innov.* **2014**, *9*, 132–140.
- [22] P. L. Anelli, L. Lattuada, V. Lorusso, M. Schneider, H. Tournier, F. Uggeri, *MAGMA* **2001**, *12*, 114–120.
- [23] a) S. Geninatti Crich, A. Deagostino, A. Toppino, D. Alberti, P. Venturello, S. Aime, *Anticancer Agents Med. Chem.* **2012**, *12*, 543–553; b) K. Takahashi, H. Nakamura, S. Furumoto, K. Yamamoto, H. Fukuda, A. Matsumura, Y. Yamamoto, *Bioorg. Med. Chem.* **2005**, *13*, 735–743; c) K. B. Gona, V. Gómez-Vallejo, D. Padro, J. Llop, *Chem. Commun.* **2013**, *49*, 11491–11493.
- [24] a) N. Cerullo, D. Bufalino, G. Daquino, *Appl. Radiat. Isot.* **2009**, *67*, S157–160; b) N. Protti, S. Geninatti Crich, D. Alberti, S. Lanzardo, A. Deagostino, A. Toppino, S. Aime, F. Ballarini, S. Bortolussi, P. Bruschi, I. Postuma, S. Altieri, H. Nikjoo, *Radiat. Prot. Dosim.* **2015**, *166*, 369–373.
- [25] a) F. Yoshida, T. Yamamoto, K. Nakai, A. Zaboronok, A. Matsumura, *Appl. Radiat. Isot.* **2015**, *106*, 247–250; b) A. Matsumura, T. Zhang, K. Nakai, K. Endo, H. Kumada, T. Yamamoto, F. Yoshida, Y. Sakurai, K. Yamamoto, T. Nose, *J. Exp. Clin. Cancer Res.* **2005**, *24*, 93–98; c) D. Alberti, N. Protti, A. Toppino, A. Deagostino, S. Lanzardo, S. Bortolussi, S. Altieri, C. Voena, R. Chiarle, S. Geninatti Crich, S. Aime, *Nanomedicine* **2015**, *11*, 741–750; d) C. Salt, A. J. Lennox, M. Takagaki, J. A. Maguire, N. S. Hosmane, *Russ. Chem. Bull.* **2004**, *53*, 1871–1888.
- [26] A. Deagostino, N. Protti, D. Alberti, P. Boggio, S. Bortolussi, S. Altieri, S. Geninatti Crich, *Future Med. Chem.* **2016**, *8*, 899–917.
- [27] S. K. Sahoo, J. Panyama, S. Prabhaa, V. Labhasetwara, S. S. Jalisatgi, *J. Controlled Release* **2002**, *82*, 105–114.
- [28] S. W. Choi, H. Y. Kwon, W. S. Kim, J. H. Kim, *Colloids Surf.* **2002**, *201*, 283–289.
- [29] A. Kumari, S. K. Yadav, S. C. Yadav, *Colloids Surf. B* **2010**, *75*, 1–18.
- [30] a) D. Alberti, M. van't Erve, R. Stefania, M. R. Ruggiero, M. Tapparo, S. Geninatti Crich, S. Aime, *Angew. Chem. Int. Ed.* **2014**, *53*, 3488–3491; *Angew. Chem.* **2014**, *126*, 3556–3559; b) U. M. Le, Z. Cui, *Int. J. Pharm.* **2006**, *312*, 105–112.
- [31] D. Feng, Y. Song, W. Shi, X. Li, H. Ma, *Anal. Chem.* **2013**, *85*, 6530–6535.
- [32] a) B. Stella, S. Arpicco, M. T. Peracchia, D. Desmaële, J. Hoebeke, M. Renoir, J. D'Angelo, L. Cattel, P. Couvreur, *J. Pharm. Sci.* **2000**, *89*, 1452–1464; b) Y. Lu, P. S. Low, *Adv. Drug Delivery Rev.* **2002**, *54*, 675–693.
- [33] F. Sonvico, C. Dubernet, V. Marsaud, M. Appel, H. Chacun, B. Stella, M. Renoir, P. Colombo, P. Couvreur, *J. Drug Delivery Sci. Technol.* **2005**, *15*, 407–410.
- [34] N. Protti, S. Manera, M. Prata, D. Alloni, F. Ballarini, A. Borio di Tigliole, S. Bortolussi, P. Bruschi, M. Cagnazzo, M. Garioni, I. Postuma, L. Reversi, A. Salvini, S. Altieri, *Health Phys.* **2014**, *107*, 534–541.

Manuscript received: January 19, 2017

Revised: February 14, 2017

Accepted Article published: February 20, 2017

Final Article published: March 16, 2017